IUST Iran University of Science and Technology

Iranian Journal of Electrical and Electronic Engineering

Journal Homepage: ijeee.iust.ac.ir

A Fast Battery Charger of Solar Vehicle with Maximum Power of Solar Cells Based on Sliding Mode Under

A. Masnabadi*, M. Asadi*(C.A.)

Abstract: This paper proposed a control system for the battery charger of a solar vehicle. The battery charger has two parts, boost converter and isolated DC/AC/DC converter. The boost converter is controlled by a proposed control system based on sliding mode. In this controller, the MPPT is implemented by an extreme point of the solar cell P-V curve. Also, the control system of the DC/AC/DC converter is based on sliding mode with consideration of uncertainties of the output filter. A fast charging algorithm based on variable frequencies was carried out by the presented control system and charging of a Lithium-ion battery was done during 20 min from SOC 20% to SOC 80%. The simulation results show control system effectiveness.

Keywords: Solar Vehicle, MPPT, Isolated DC/AC/DC Converter Sliding Mode Control, Uncertainties of the Filter.

Nomnclature

Symbol	Description
I_{Ph}	composed of a photocurrent generator source
R_S	series resistance
R_{Sh}	shunt resistance
V_{PV}	output voltage of solar
q	electron charge ($1.602 \cdot 10^{-19}$ C)
γ	ideality factor
k	Boltzmann constant ($1.381 \cdot 10^{-23}$ J/K)
T	Cell and reference temperatures (K)
Ncell	Number of cells in series
K_i	temperature coefficient of Isc (A/K)
T_{ef}	Cell and reference temperatures (K)
β, β_{ref}	Solar and reference irradiances (W/m2)
I_{SC}	Short-circuit current (A)
I_{Or}	reverse current of the cell (A)
E_G	Band gap
C_b	Output filter capacitor of boost converter
L_b	Output filter inductor of boost converter
C	Output filter capacitor of DC-DC converter
L	Output filter inductor of DC-DC converter
V_{dc}	Input voltage of DC-DC converters
V_{OC}	Open circuit voltage of battery
R_i:	Internal resistance of the battery
L_L	Transformer leakage inductor
f_{sw}	Switching frequency

Iranian Journal of Electrical & Electronic Engineering, 2024.
Paper first received 9 Jan 2023 and accepted 18 March 2024.
* The authors are with the Department of Electrical Engineering, Arak University of Technology, Arak, Iran.
E-mail: abolfazl.masnabadi73@gmail.com.

E-mails: m.asadi@arakut.ac.ir,
Corresponding Author: M.Asadi.

n	Transformer ratio
V_{cb}^{*}	Reference voltage of boost converter
P_b	Power delivered to the battery
i_L^{*}	Reference currents of DC-DC converter
$\mathrm{i_L}$	Actual currents of DC-DC converter

1 Introduction

THE solar vehicles can decrease city pollution [1]. Due to the use of solar systems in these devices, these systems have disadvantages such as low performance of the PV module and nonlinear behavior characteristic of PV cell voltage [2]. In order to solve these problems, different solutions have been proposed to improve the performance of PV. One of the most important solutions offered is MPPT techniques which can be referred to [3],[4]. The Perturb and Observer (P&O) method is used in many cases to obtain MPPT. The P&O method has a simple algorithm but has oscillation around the maximum power [5],[6].

In order to improve the MPPT algorithms, artificial genetic algorithms [7] and intelligence methods [8],[9] have been proposed too. These techniques are highly superior in terms of MPPT tracking because they immediately reach maximum power without considering sudden changes in weather conditions and without fluctuations in steady state [10]. But the mentioned methods have complexed calculations.

Many control methods have been proposed for battery charging. One of these methods is sliding mode control method. Due to the advantages of Sliding Mode Control (SMC) such as fast response and simplicity, this controller has been used in most PV systems [11], [12]. In [13], the SMC is used to control the inverter to the measured current follow the reference current.

One of the important parts of the solar vehicle is chargeable battery. So, the fast battery chargers are important in the electric transportation. Different states of charge are given in [14] Current Control (C-C) and Constant Voltage (C-V) charging method is very popular because of its simplicity and safety [15], [16]. The C-C and the C-V charging methods are not fast. For fast charging using C-C, the charging current amplitude must be around 1.8 times of battery rated current. This can increase battery life. Recently, the sinusoidal charging method has shown considerable performance. This method of charging increases the battery charging performance via minimizing battery impedance, and causes charging of battery in much shorter time than the constant current-constant voltage method [17], [18].

Different controllers can be used in the battery charging system. One of the simplest controllers is the PI controller. This controller is suitable for charging the battery with the constant current method, but the ability of this controller to cover uncertainties is lower than other controllers. Also, in nonlinear system this controller is not capable of tracking at different frequencies due to constant coefficients [19]. Therefore, in [20], a state-space based controller is designed in which the reference signal is tracked with acceptable accuracy at different frequencies. Also, in [21], an adaptive PI controller based on Model Reference Adaptive Control has been introduced to be able to adjust the variable frequency of the charging wave current and the problem of accurate current detection at different frequencies has been solved.

In [22], [23], fuzzy controllers, neural networks, genetic algorithms and predictive models for battery charging are examined. But implementing of these controllers is highly complex and costly.

In [20] a control system for charging the sinusoidal current of lithium-ion batteries is presented. In this method, a combination of DC current and sinusoidal current is injected into the battery. By selecting the optimal frequency, the AC impedance of the battery is minimized, which low impedance increases the battery charging speed.

In this paper, in order to achieve maximum power from the solar cell by changing the weather to control, a sliding mode controller has been used. Climate changes is considered a disturbance. Since the sliding mode controller is robust, it can cover these disturbances. In order to design the proposed battery charger controller, in the trickle charging stage, the constant current-constant voltage charging steps are used, and for fast battery charging, a combination of DC current and sinusoidal charging method is applied to the battery. In the practice, Due to aging; there are changes in inductance and capacitance of output filter. The proposed sliding mode controller can solve this problem in this paper.

This paper presents a control system to obtain maximum power under uncertainty of output filter inductor and capacitor. The references [14-16] present control system under modes CC and CV, and this paper completes these modes under uncertainty. In addition, this paper covers the CC and CV modes under sinusoidal injection to achieve fast charging in comparing with [17] and [18].
The rest of the paper is organized as follows: Section 2 presents the configuration and modelling of solar cell and battery charger, Section 3 deals with SMC design of boost converter, constant current and constant voltage, uncertainty of inductor and capacitor parameters of output filter are given in Section 4. Simulation results of solar cell and battery charger and conclusions are provided in Section 5 and 6 respectively.

2 Configuration and Modelling of Solar Cell and Battery Charger

Fig.1 shows a solar vehicle. This vehicle consists of a solar cell, MPPT, boost converter, and battery charger that consists of full-bridge DC-DC converter, a battery, Battery Management System (BMS) and control system. It also includes a SMC to control the boost converter and the full bridge DC-DC convertor, according to the current and voltage references provided by the BMS.1 shows a solar vehicle. This vehicle consists of a solar cell, MPPT, boost converter, and battery charger that consists of full-bridge DC-DC converter, a Battery, a Battery Management System (BMS) and control system. It also includes a SMC to control the boost converter and the full bridge DC-DC convertor, according to the current and voltage references provided by the BMS.

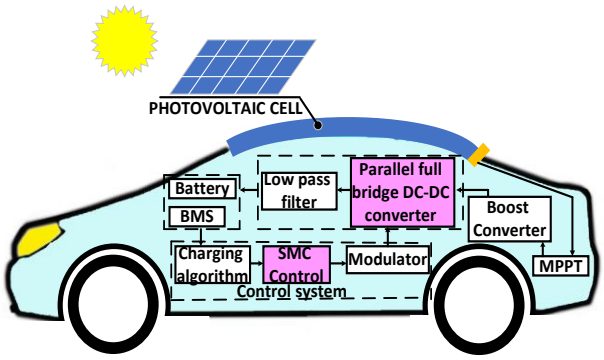

Fig. 1 Schematic of solar vehicle.

3 Mathematical Modelling of the Solar Cell

Fig. 2 shows a popular model of a solar cell. This model is good performance in the presence of high changes of irradiance and temperature [24].

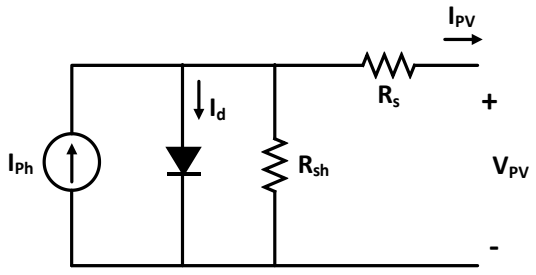

Fig. 2 Popular model of a solar cell.

By applying KVL and KCL laws, the output current Ipv is expressed by the following equation [24]:

$$I_{PV} = \mathrm{I}_{Ph} - \mathrm{I}_{OS}[\exp(A_C(\mathrm{V}_{PV} + \mathrm{R}_S\mathrm{I}_{PV}) - 1)] - \frac{\mathrm{V}_{PV} + \mathrm{R}_S\mathrm{I}_{PV}}{\mathrm{R}_{Sh}} \quad (1)$$

Where: $A_C = \frac{\mathrm{q}}{\gamma \mathrm{kTNcell}}$.

The measured current I_{PV} depends on temperature and radiation by the following equation [24]:

$$I_{PV} = \mathrm{K}_i(T - \mathrm{T}_{ref})\frac{\beta}{\beta_{ref}} + \mathrm{I}_{SC} \quad (2)$$

I_{OS} is saturated current and is defined as (3) [24].

$$I_{OS} = \mathrm{I}_{Or}(\frac{T}{\mathrm{T}_{ref}})^3 + \exp(\frac{qE_G}{K\gamma}[\frac{1}{T} - \frac{1}{\mathrm{T}_{ref}}]) \quad (3)$$

4 Control System Design

Fig. 3 shows the power system of the boost converter, and battery charger. In this figure (Fig. 3), there are four state variables $x_1 = i_{Lb} = i_{PV}$, $x_2 = V_{Cb} = V_{dc}$, $x_3 = i_L$ and $x_4 = V_C$. After simplification, the state-space equation of boost converter and full-bridge DC-DC converter can be obtained as (4) and (5) respectively.

$$\begin{bmatrix}\dot{x_1}\\ \dot{x_2}\end{bmatrix} = \begin{bmatrix}0 & -\frac{(1-\alpha)}{L_b}\\ \frac{(1-\alpha)}{C_b} & -\frac{1}{R_{th}C_b}\end{bmatrix}\begin{bmatrix}x_1\\ x_2\end{bmatrix} + \begin{bmatrix}\frac{1}{L_b}\\ 0\end{bmatrix}V_{PV}. \quad (4)$$

$$\begin{bmatrix}\dot{x_3}\\ \dot{x_4}\end{bmatrix} = \begin{bmatrix}-\frac{R_{eq}}{L} & -\frac{1}{L}\\ \frac{1}{C} & -\frac{1}{R_iC}\end{bmatrix}\begin{bmatrix}x_3\\ x_4\end{bmatrix} + \begin{bmatrix}\frac{2nV_{dc}}{L}\\ 0\end{bmatrix}d + \begin{bmatrix}0\\ \frac{1}{R_iC}\end{bmatrix}V_{OC} \quad (5)$$

R_{eq} is calculated according to (6) [25] and Rth is calculated by (7) too.

$$R_{eq} = 2L_L n^2 f_{sw} \quad (6)$$

$$R_{th} = \frac{V_{cb}^*}{P_b} \quad (7)$$

4.1 Control system of boost converter

In order to achieve high power of the solar cell at low temperatures and low radiation, the control system is designed to receive high power from the cell in these conditions.

For this purpose, in the sliding mode controller, the surface is defined as the following equation:

$$S_b = \mathrm{e}_b + \lambda_b \int \mathrm{e}_b \, \mathrm{dt} \quad (8)$$

Where λb is coefficients of sliding mode surface of boost converter and eb is the ratio of the rate of change of power to the change in voltage of the solar cell is defined as (9).

$$e_b = \frac{dP_{PV}}{dV_{PV}} \quad (9)$$

where $P_{PV} = V_{PV} x_1$ (10)

By substitution of (9) in (10) can be written:

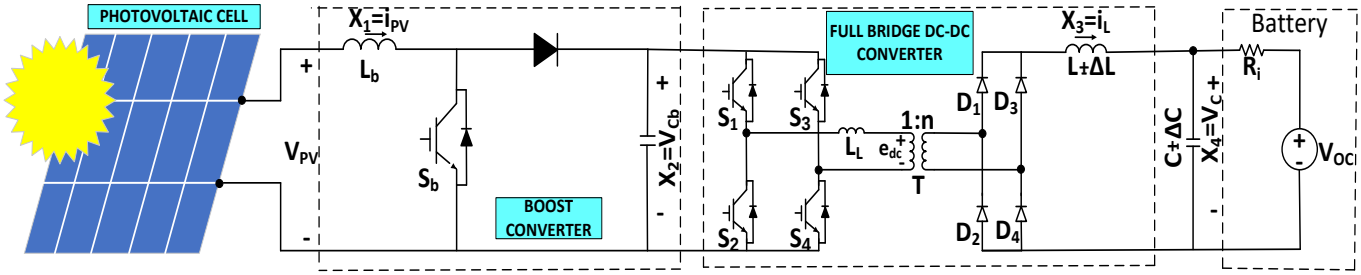

Fig. 3 The power system of the boost converter and battery charger

$$e_b = \frac{dP_{PV}}{dV_{PV}} = x_1 + V_{PV}\frac{dx_1}{dV_{PV}} \quad (11)$$

By derivation of the equations (8), it can be expressed as:

$$\dot{S_b} = \dot{e_b} + \lambda_b e_b \quad (12)$$

Where:

$$\dot{e_b} = \frac{de_b}{dt} = \frac{dx_1}{dt} + \frac{d}{dt}(V_{PV}\frac{dx_1}{dV_{PV}}) \quad (13)$$

And:

$$\frac{dx_1}{dV_{PV}} = \frac{-A_C I_{OS}\exp[A_C(V_{PV}+R_S I_{PV})-1] - 1/R_{Sh}}{R_S A_C I_{OS}\exp[A_C(V_{PV}+R_S I_{PV})-1] + R_S/R_{Sh} + 1} \quad (14)$$

The definite positive potential functions can be defined as:

$$W_b = \frac{1}{2}{S_b}^2 \quad (15)$$

In order for asymptotic stability, the derivation of W_b must be negative.

$$\dot{W_b} = \dot{S_b} S_b < 0 \quad (16)$$

Where in:

$$\dot{S_b} = -K_b sign(S_b) \quad (17)$$

K_b should be positive.

Also, in order to control the voltage in the boost converter, the voltage error is defined as follows:

$$e_{bV} = x_2^* - x_2 \quad (18)$$

By derivation of (17), can be written as:

$$\dot{e_{bV}} = \dot{x_2^*} - \dot{x_2} \quad (19)$$

By substitution of (18) and (19) in (4), can be written as:

$$\dot{e_{bV}} + \left(\frac{1}{R_{th}C_b} + k_C\right) e_{bV} = 0 \quad (20)$$

In (20) must: $k_C > -\frac{1}{R_{th}C_b}$

Where:

$$k_C e_{bV} = -\dot{x_2^*} + \frac{(1-\alpha)}{C_b} x_1 - \frac{1}{R_{th}C_b} x_2^* \quad (21)$$

Because the reference voltage (x_2^*) is a constant value, then $\dot{x_2^*} = 0$.

After simplification, the x_1 can be obtained as (21):

$$x_1 = \frac{C_b k_C e_{bV} + x_2^*/R_{th}}{1-\alpha} \quad (22)$$

By substitution of (11), (13) and (22) in (12), after simplification can written as:

$$\alpha = 1 - \frac{C_b k_C e_{bV} + x_2^*/R_{th}}{B} \quad (23)$$

Where:

$$B = -\int (K_b sign(S_b) + \frac{d}{dt}\left(V_{PV}\frac{dx_1}{dV_{PV}}\right) + \lambda_b e_b)dt \quad (24)$$

The block diagram of this control system Shown in Fig. 4.

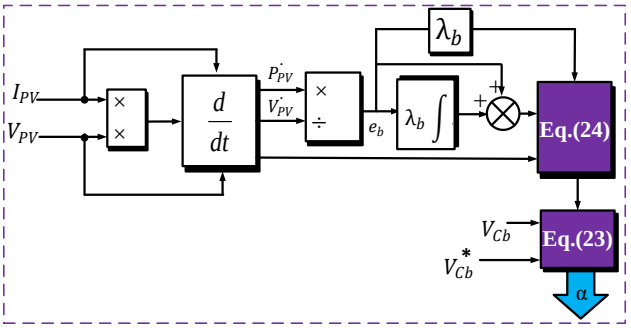

Fig. 4 The control system of the boost converter

4.2 Control system of battery charger

The proposed control system for battery charging has two stages: C-C mode and C-V mode. The current control mode consists of two stages: trickle mode with $0.1C_{batt}$ (C_{batt} is Battery capacity) and sinusoidal mode with $1C_{batt}$ offset. In order to prevent overcharging of the battery and to limit the charging current is used the

constant voltage mode. Algorithm of charging battery is shown in Fig. 7 [20]. It has two steps. In the first step, voltage and temperature of battery are measured respectively. In the second step, there are three charge modes according to the battery voltage. If battery voltage is between 36V to 43.5V, trickle charging is selected, it means, the battery is charging with $0.1C_{batt}$. If voltage is between 40 V to 43.5V, sinusoidal charging is applied to the battery. If battery voltage equals to 43.2 V, battery is charged with constant voltage algorithm.

This paper uses the sliding mode control for control of C-C and C-V mode of battery charger.

4.3 Control system of C-C mode

In C-C mode of charge to minimize the steady state error chattering and to improve the transient response is employed for sliding surface as (25).

$$S_1 = \mathrm{e}_1 + \lambda_1 \int \mathrm{e}_1 \,\mathrm{dt} + \lambda_2 \int\int \mathrm{e}_1 \,\mathrm{dt} \tag{25}$$

Where S_1 is sliding mode surface of C-C mode and e_1 are error between reference current and the actual current of converter. λ_1 and λ_2 are coefficients of sliding mode surface of C-C mode.

The errors can be written as:

$$e_1 = i_{\mathrm{L}}^{*} - i_L \tag{26}$$

By derivation of the equations (25) and (26), they can be expressed as:

$$\dot{S_1} = \dot{e_1} + \lambda_1 e_1 + \lambda_2 \int \mathrm{e}_1 \,\mathrm{dt} \tag{27}$$

$$\dot{e_1} = \dot{\imath_{\mathrm{L}}^{*}} - \dot{\imath_L} \tag{28}$$

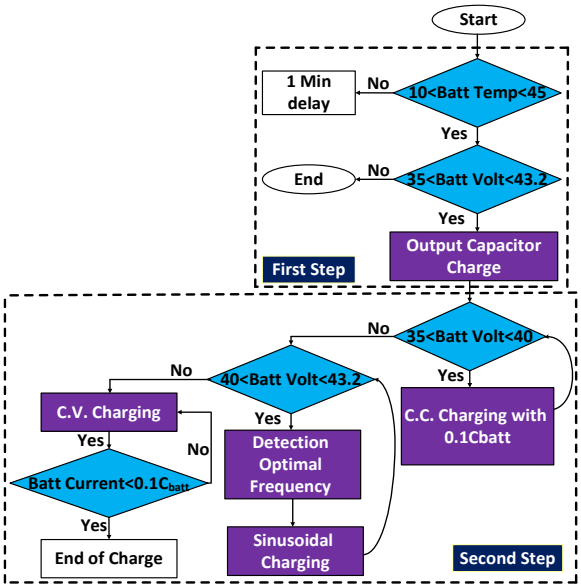

Fig. 5 The power system of the boost converter and battery charger

By substitution of (28) and Eq. (5) in (27), can be written:

$$\dot{S_1} = \begin{bmatrix} \dot{\imath_L^{*}} - \left(\frac{2dn}{L} V_{dc} - \frac{1}{L} V_c - \frac{R_{eq}}{L} i_L\right) \\ +\lambda_1 (i_L^{*} - i_L) + \lambda_2 \int (i_L^{*} - i_L) \,\mathrm{dt} \end{bmatrix} \tag{29}$$

The Lyapunov theorem can be employed for extracting of duty cycle d. The definite positive potential functions can be defined as:

$$W_1 = \frac{1}{2} {S_1}^2 \tag{30}$$

In order for asymptotic stability, the derivation of W_1 must be negative.

$$\dot{W_1} = \dot{S_1} S_1 < 0 \tag{31}$$

Where in:

$$\dot{S_1} = -Ksign(S_1) \tag{32}$$

K is coefficient of Lyapunov theorem in C-C mode. K should be positive.

By substituting (32) in (29) and simplifying the equations, d can be calculated as:

$$d = \frac{L}{2nV_{dc}} \begin{bmatrix} \frac{R_{eq}}{L} i_L + \lambda_1 (i_L^{*} - i_L) + \lambda_2 \int (i_L^{*} - i_L) \,\mathrm{dt} \\ +\dot{\imath_L^{*}} + \frac{1}{L} V_c + Ksign(S_1) \end{bmatrix} \tag{33}$$

Where d is duty cycle of DC-DC converter and V_C is Actual voltage of DC-DC converters.

4.4 Uncertainty of The Output Filter in C-C mode

In this section, the changes of the parameters of the full bridge DC-DC converter, such as inductor and capacitor of output filter, are considered. The changes in the parameters can be increased or decreased during the work. The control system should compensate these changes. The changes of inductor and capacitor of output filter can be modeled as (34) and (35) respectively.

$$L \pm \Delta L \tag{34}$$

$$C \pm \Delta C \tag{35}$$

Where ΔLis changes of output filter inductor and ΔC is changes of output filter capacitor.

After substitution of (34) and (35) in (33) and simplification, (36) can be approximated as follows:

$$2nV_{dc}d = \begin{bmatrix} \begin{bmatrix} L\lambda_1 (i_L^{*} - i_L) + L\lambda_2 \int (i_L^{*} - i_L) \,\mathrm{dt} \\ R_{eq} i_L + L\dot{\imath}_L^{*} + V_c + KLsign(S_1) \end{bmatrix} \\ \pm \Delta L \lambda_1 (i_L^{*} - i_L) \\ \pm \Delta L \lambda_2 \int (i_L^{*} - i_L) \,\mathrm{dt} \\ \pm \Delta L \dot{\imath}_L^{*} \pm K \Delta L sign(S_1) \end{bmatrix} \tag{36}$$

Considering (31), the changes can be defined as:

$$H_1 = \begin{bmatrix} \pm\Delta L\lambda_1(i_L^* - i_L) \pm \Delta L\lambda_2 \int (i_L^* - i_L)\,\mathrm{dt} \\ \pm\Delta L\dot{i_L^*} \pm K\Delta L sign(S_1) \end{bmatrix} \quad (37)$$

For the system robustness, the (37) must be satisfied:

$$\max(H_1) \ll KLsign(S_1) \quad (38)$$

Sign (S_1) can be +1 or -1. So can be written:

$$\max(H_1)/L \ll |K| \quad (39)$$

Fig. 6-a shows the block diagram of duty cycle extraction in C-C mode.

4.5 Controller system of C-V mode

In this mode, the voltage must be controlled, so the sliding surfaces of this mode can be defined as (40).

$$S_2 = \dot{e_2} + \gamma_1 e_2 + \gamma_2 \int \mathrm{e}_2\,\mathrm{dt} \quad (40)$$

Where S_2 is sliding mode surface of C-V mode, γ_1, γ_2 are coefficients of sliding mode surface of C-V mode and e_2, *is* defined as (41).

$$e_2 = V_C^* - V_C \quad (41)$$

Where V_C^* is reference voltage of DC-DC converter and V_C Actual voltage of DC-DC converters. By derivation of (40) and substituting (41), in them, can be written as:

$$\dot{S_2} = -\dot{V_C} - \gamma_1\dot{V_C} + \gamma_2(V_C^* - V_C) \quad (42)$$

In order for asymptotic stability, the derivation of W_2 must be negative:

$$\dot{W_2} = \dot{S_2}S_2 < 0 \quad (43)$$

$$\dot{S_2} = -K'sign(S_2) \quad (44)$$

$K'$is coefficient of Lyapunov theorem in C-V mode. K' should be positive.

By substituting (5) in (42) and simplifying the equations, the duty cycle can be obtained as:

$$d = \frac{L}{2nV_{dc}} \begin{bmatrix} \gamma_2 V_C^* + \left(\frac{R_{eq}}{LC} + \frac{(1-\gamma_1 R_i)}{R_i C}\right) i_L \\ + \left(\frac{1}{LC} - \frac{(1-\gamma_1 R_i)}{{R_i}^2 C} - \gamma_2\right) V_c \\ + \frac{(1-\gamma_1 R_i)}{{R_i}^2 C} V_{OC} + k'sign(S_2) \end{bmatrix} \quad (45)$$

4.6 Uncertainty of The Output Filter in C-V Mode

At this stage, uncertainties are considered as in Section 3-4. Substituting of (34) and (35) in (45), it can be written as (46).

$$2nV_{dc}d = \begin{bmatrix} \begin{bmatrix} \gamma_2 V_C^* + \left(\frac{R_{eq}}{LC} + \frac{(1-\gamma_1 R_i)}{R_i C}\right) i_L \\ + \left(\frac{1}{LC} - \frac{(1-\gamma_1 R_i)}{{R_i}^2 C} - \gamma_2\right) V_c \\ \frac{(1-\gamma_1 R_i)}{{R_i}^2 C} V_{OC} + k'sign(S_2) \end{bmatrix} \\ (\pm\Delta C, L \pm \Delta L, C)\gamma_2 V_C^* \\ \pm\Delta L, i_L\left(\frac{1-\gamma_1 R_i}{R_i}\right) \\ \pm\Delta L(V_{OC} + V_c)\left(\frac{1-\gamma_1 R_i}{{R_i}^2}\right) \\ \pm\Delta C, \gamma_2, V_c \\ k'(\pm\Delta C, L \pm \Delta L, C)sign(S_2) \end{bmatrix} \quad (46)$$

The changes part of (46) can be approximated as (47).

$$H_2 = \begin{bmatrix} (\pm\Delta C, L \pm \Delta L, C)\gamma_2 V_C^* \\ \pm\Delta L, i_L\left(\frac{1-\gamma_1 R_i}{R_i}\right) \\ \pm\Delta L(V_{OC} + V_c)\left(\frac{1-\gamma_1 R_i}{{R_i}^2}\right) \\ \pm\Delta C, \gamma_2, V_c \\ k'(\pm\Delta C, L \pm \Delta L, C)sign(S_2) \end{bmatrix} \quad (47)$$

For the system robustness, the (47) must be satisfied.

$$\max(H_2) \ll k'Lsign(S_2) \quad (48)$$

Sign (S_2) can be +1 or -1. So can be written:

$$\max(H_2)/L \ll |k'| \quad (49)$$

In Fig. 6 has been shown the block diagram of duty cycle extraction in C-V mode.

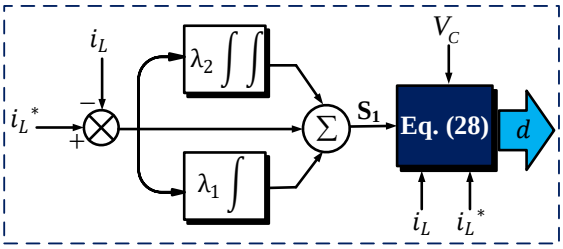

a) Control system of C-C mode

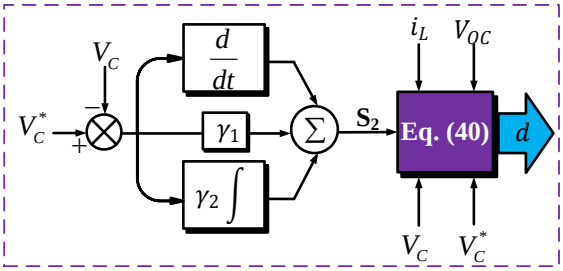

b) Control system of C-V mode

Fig. 6 The control system of the boost converter

5 Structure of control system

Complete schematic diagram of the solar Vehicle is

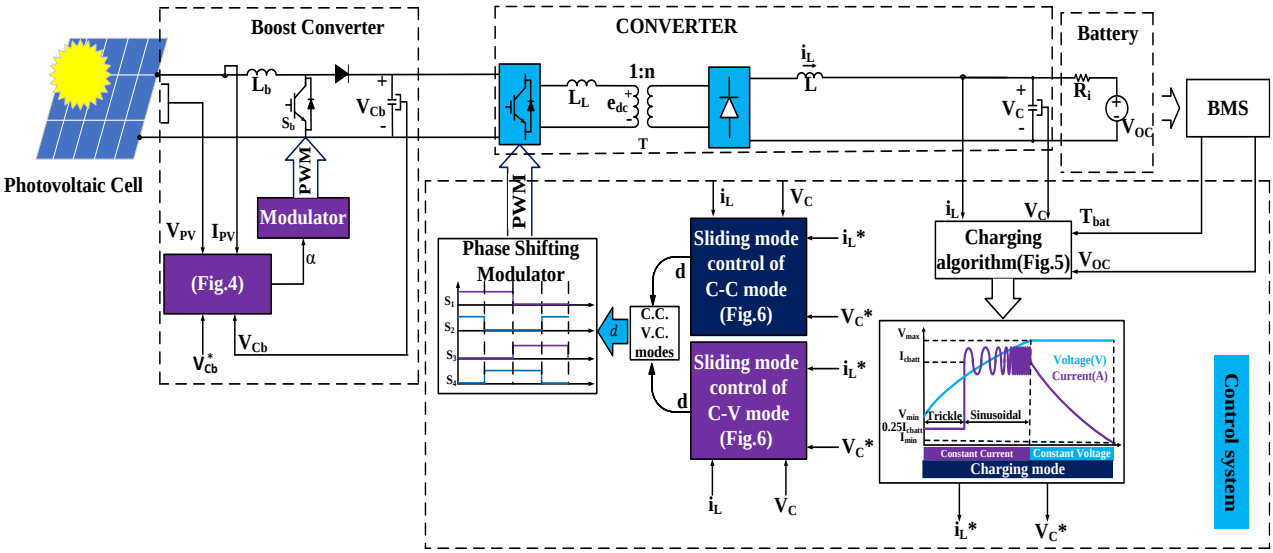

Fig. 7 The control system of the boost converter

shown in Fig. 8. In this figure, the output voltage of boost converter, the voltage and current of PV after measuring are sent to the control system according equations section 3.1. After calculating the duty cycle (α), to generate the converter pulse, duty cycle is provided for the modulator unit.

The situation is the same in the converter of battery charger. In this converter, the parameter of battery such as V_{oc} and T_{batt} are transmitted from BMS to the charging algorithm. After measuring the terminal voltage, the algorithm selects one of the two charging processes and two reference are calculated. This reference values including inductor current (i_L^*), capacitor voltage (V_C^*). To calculate the converter duty cycle (d), reference and measured values are used in the sliding mode control according to the equations in section 3-3 and 3-5. In order to make the converter switching pulse, duty cycle is provided for the phase shifting modulator unit. Finally, the PWM pulses are applied to the converter.

6 Simulation Results

The parameters of solar cells and converters are given in Table 1 and simulations are performed in Simulink / MATLAB. The simulation files can be found through "https://drive.google.com/file/d/1lrrq87oWxhYBfN9OBql__7Hc_QipfChc/view?usp=sharing".

6.1 Results of solar cell and boost converter

The value of the converter output voltage is considered as the reference voltage, 600v (Fig.8-c). As shown in Fig.8-a when the amount of radiation on the solar cell decreases, also the power of solar cell decreases (Fig.8-b), but the control system increases the duty cycle applied to the boost converter to counteract this reduction (Fig.8-d), as a result, after power reduction, it quickly reaches its maximum value. By increasing the amount of radiation, the results will be the opposite.

With increasing ambient temperature, unlike the previous case, the output power should decrease, in which case the duty cycle increases.

6.2 Results of charging the Li-ion battery

Output current of the battery during complete charge shown in Fig. 9. This figure shows the three steps of battery charging. In the first step, the battery is charging with trickle charge and current value is 0.25 C_{batt}. This step is slow and that has increased the charging time. In the second step, a combination of DC current and sinusoidal current is injected into the battery. In this step, Lithium-ion battery is charged by a sinusoidal current with 10+4sin(2πf). The method of calculating the sinusoidal current frequency is given in [18]. Finally, in the third step, the battery is charging with C-V mode. In this step, battery voltage reach to 43.5v and battery current decreased to 0.1 C_{batt}.

In these three steps, the Battery voltage increase from 36 v to nominal value 43.5 that is shown in Fig. 10.

The State of Charge (SOC) of the battery as shown in Fig. 11. It has been increased from 5% to 20% in about 35 min but that has been increased from 20% to 80% in about 26 minutes. Due to the charging time and the amount of SOC, the charging speed is much higher in the sinusoidal stage. The calculation of SOC is given in [26].

Table 1 The parameter of the converter, battery and sliding mode controller coefficients

	Symbol and unit	Parameters	Values
The parameters of solar cell	N_{Cell}	Number of cells in series	36
	$P_{mpp}(W)$	Power	55
	$V_{mpp}(V)$	Voltage	27.32
	$I_{mpp}(A)$	Current	9.15
	$V_{OC}(V)$	Open circuit voltage	34.19
	$I_{sc}(A)$	Short circuit current	10
	$K_i(A/K)$	Temperature coefficient of Isc	0.0004
The parameters of the boost Converter	$f_{swb}(KHz)$	Switching frequency	15
	$C_b(\mu F)$	Capacitor	1.8
	$L_b(mH)$	Inductor	1.65
The parameters of the Full Bridge DC-DC Converter	$f_{sw}(KHz)$	Switching frequency	15
	$L(mH)$	Output filter inductor	2.77
	C(μF)	Output filter capacitor	2.5
	$L_L(\mu H)$	Transformer leakage inductor	20
	$n_1:n_2$	Transformer ratio	3:1
The parameters of the Li-ion battery	$C_{batt}(A.h)$	Battery capacity	10
	$i(A)$	Maximum charge current	10
	$V(v)$	Full charge voltage	43.5
	$V(v)$	Full discharge voltage	36
	$R_i(m\Omega)$	Electrolyte resistance	183.6

6.3 Uncertainty of C-C and C-V modes simulations

In inductor and capacitor are changed because of a fault or temperature changes. These changes shown in battery voltage and battery current. These changes are shown in Fig. 12 and 13 as a 20% increase or decrease in the voltage and current of the full bridge DC-DC converter. For example, when the capacitor increases, the current passing through the inductor increases, in which case the control system reduces the amount of duty cycle(d) applied to the full bridge DC-DC converter to prevent the inductor current from increasing.

7 Conclusion

A control system for the battery charger of a solar vehicle was presented in this paper. A state-space equation of boost converter and charger were extracted in this paper too. The simulation result of the presented control method shows that the reference signals tracking was effectively done under changing of the amount of radiation and temperature on the solar cell and uncertainties of output filter of the charger in current control and voltage control modes. Also, a fast charging algorithm based on variable frequencies was carried out by the presented control system and charging of a Lithium-ion battery was done during 20 min from SOC 20% to SOC 80%.

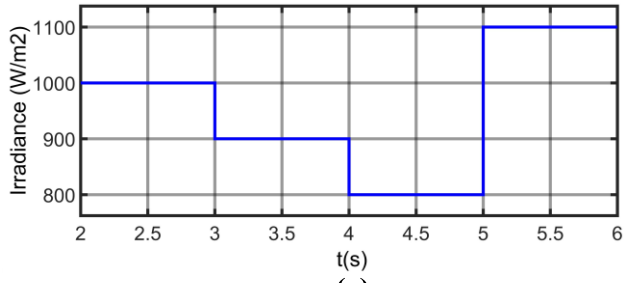

(a)

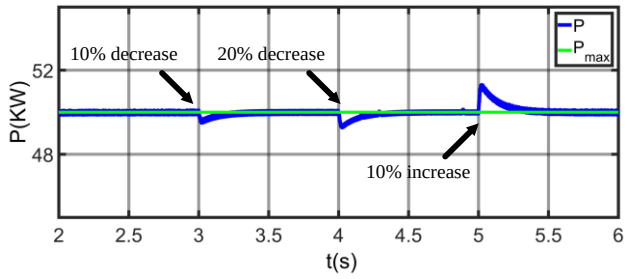

(b)

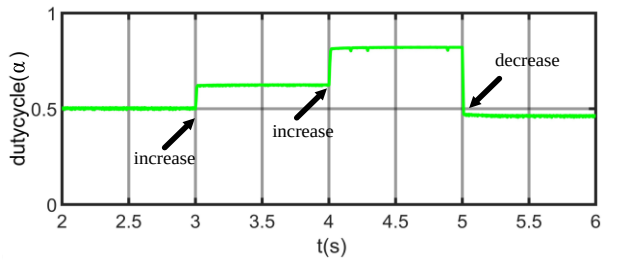

(d)

Fig. 8 Parameters of solar cell a) Irradiance, b) Output power, c) Duty cycle

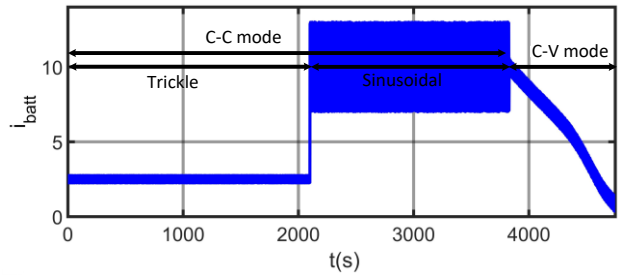

Fig. 9 Li-ion battery charging current in complete charge

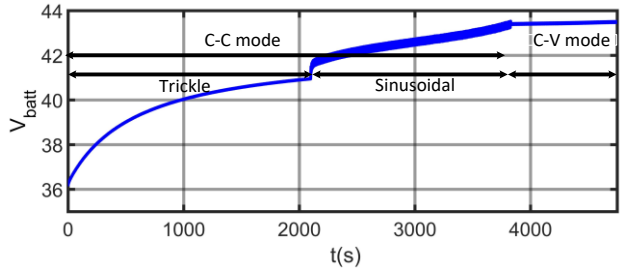

Fig. 10 Li-ion battery charging voltage in complete charge

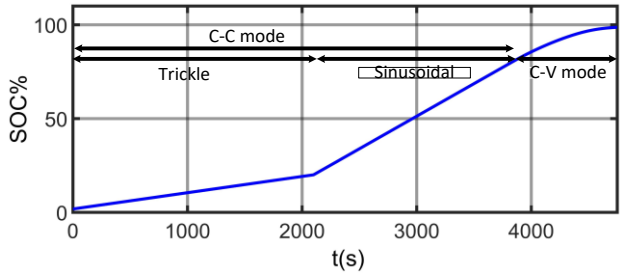

Fig. 11 Li-ion battery charging SOC in complete charge

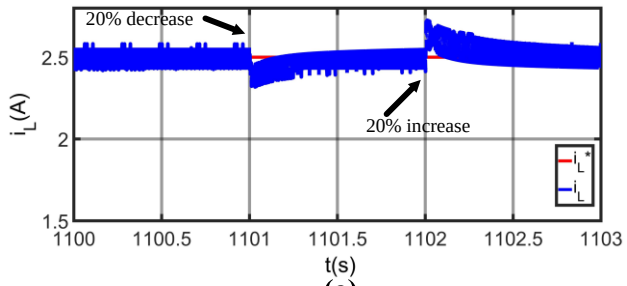

(a)

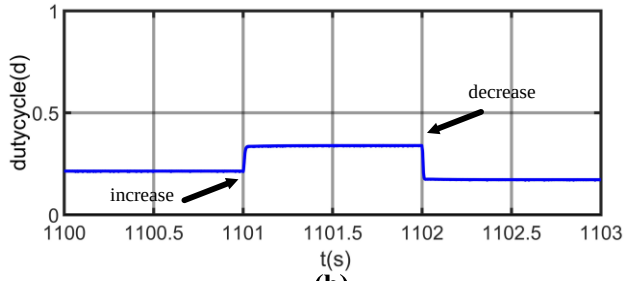

(b)

Fig. 12 a) Full bridge converter current, b) Duty cycle

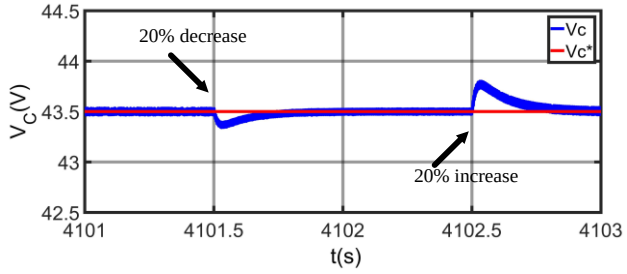

(a)

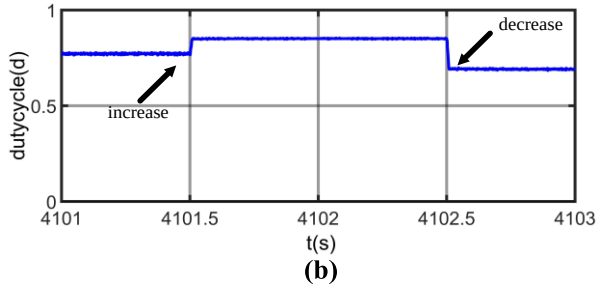

(b)

Fig. 13 a) Capacitor voltage, b) Duty cycle

References

[1] Tolga Ercan, Nuri C. Onat, Nowreen Keya, Omer Tatari, Naveen Eluru, Murat Kucukvar, Autonomous electric vehicles can reduce carbon emissions and air pollution in cities, Transportation Research Part D: Transport and Environment, Volume 112, 2022, 103472, ISSN 1361-9209.

[2] S. Drid, L. Chrifi-Alaoui, P. Bussy, and M. Ouriagli, "Robust control of the photovoltaic system with improved maximum power point tracking," in 2014 Ninth International Conference on Ecological Vehicles and Renewable Energies (EVER), 2014, pp. 1-7: IEEE.

[3] J. Hahm, J. Baek, H. Kang, H. Lee, and M. Park, "Matlab-based modeling and simulations to study the performance of different MPPT techniques used for photovoltaic systems under partially shaded conditions," International Journal of Photoenergy, vol. 2015, 2015.

[4] D. Verma, S. Nema, A. Shandilya, and S. K. Dash, "Maximum power point tracking (MPPT) techniques: Recapitulation in solar photovoltaic systems," Renewable and Sustainable Energy Reviews, vol. 54, pp. 1018-1034, 2016.

[5] N. Femia, D. Granozio, G. Petrone, G. Spagnuolo, and M. Vitelli, "Predictive & adaptive MPPT perturb and observe method," IEEE Transactions on Aerospace and Electronic Systems, vol. 43, no. 3, pp. 934-950, 2007.

[6] J. Ahmed and Z. Salam, "An improved perturb and observe (P&O) maximum power point tracking (MPPT) algorithm for higher efficiency," Applied Energy, vol. 150, pp. 97-108, 2015.

[7] A. A. Kulaksız and R. Akkaya, "A genetic algorithm optimized ANN-based MPPT algorithm for a stand-alone PV system with induction motor drive," Solar Energy, vol. 86, no. 9, pp. 2366-2375, 2012.

[8] C. B. Salah and M. Ouali, "Comparison of fuzzy logic and neural network in maximum power point tracker for PV systems," Electric Power Systems Research, vol. 81, no. 1, pp. 43-50, 2011.

[9] N. A. Gounden, S. A. Peter, H. Nallandula, and S. Krithiga, "Fuzzy logic controller with MPPT using line-commutated inverter for three-phase grid-connected photovoltaic systems," Renewable Energy, vol. 34, no. 3, pp. 909-915, 2009.

[10] M. M. Zainuri, M. M. Radzi, A. C. Soh, and N. A. Rahim, "Adaptive P&O-fuzzy control MPPT for PV boost dc-dc converter," in *2012 IEEE International Conference on Power and Energy (PECon)*, 2012, pp. 524-529: IEEE.

[11] I.-S. Kim, "Robust maximum power point tracker using sliding mode controller for the three-phase grid-connected photovoltaic system," *Solar energy*, vol. 81, no. 3, pp. 405-414, 2007.

[12] S. Dhar and P. Dash, "A finite time fast terminal sliding mode I–V control of grid-connected PV array," *Journal of Control, Automation and Electrical Systems*, vol. 26, no. 3, pp. 314-335, 2015.

[13] I.-S. Kim, M.-B. Kim, and M.-J. Youn, "New maximum power point tracker using sliding-mode observer for estimation of solar array current in the grid-connected photovoltaic system," *IEEE Transactions on industrial Electronics*, vol. 53, no. 4, pp. 1027-1035, 2006.

[14] S. Inamdar, A. Thosar, and S. Mante, "Literature review of 3.3 kW on board charger topologies," in 2019 3rd International conference on Electronics, Communication and Aerospace Technology (ICECA), 2019, pp. 276-281: IEEE.

[15] R. C. Cope and Y. Podrazhansky, "The art of battery charging," in Fourteenth Annual Battery Conference on Applications and Advances. Proceedings of the Conference (Cat. No. 99TH8371), 1999, pp. 233-235: IEEE.

[16] T. Instruments, "Simple CC/CV charger using TPS54331," Application Note, SLVA551-December, 2012.

[17] L.-R. Chen, "Design of duty-varied voltage pulse charger for improving Li-ion battery-charging response," IEEE Transactions on Industrial Electronics, vol. 56, no. 2, pp. 480-487, 2008.

[18] L.-R. Chen, S.-L. Wu, D.-T. Shieh, and T.-R. Chen, "Sinusoidal-ripple-current charging strategy and optimal charging frequency study for Li-ion batteries," IEEE Transactions on Industrial Electronics, vol. 60, no. 1, pp. 88-97, 2012.

[19] Pavković, Danijel & Lobrovic, Mihael & Hrgetic, Mario & Komljenović, Ante & Smetko, Viktor. (2014). Battery Current and Voltage Control System Design with Charging Application. 10.1109/CCA.2014.6981481.

[20] H. Vazini, M. Asadi, M. Karimadini, and H. Hajisadeghian, "Sinusoidal charging of Li-ion battery based on frequency detection algorithm by pole placement control method," IET Power Electronics, vol. 12, no. 3, pp. 421-429, 2019.

[21] J.-G. Chen, Y.-D. Lee, and S.-Y. Park, "Adaptive PI gain control to realize sinusoidal ripple current charging," in 2015 9th International Conference on Power Electronics and ECCE Asia (ICPE-ECCE Asia), 2015, pp. 2582-2589: IEEE.

[22] T. N. Mai, M. Shcherbakov, T. Q. Vinh, N. Shcherbakova, and V. Kamaev, "Hybrid renewable energy systems control based on predictive models and genetic algorithms," Creativity in Intelligent Technologies and Data Science (CIT&DS 2015),

Volgograd, Russia, pp. 515-527, 2015.
[23] C.-H. Cheng and J.-X. Ye, "GA-based neural network for energy recovery system of the electric motorcycle," Expert Systems with Applications, vol. 38, no. 4, pp. 3034-3039, 2011.
[24] Y. Chaibi, M. Salhi, and A. El-Jouni, "Sliding mode controllers for standalone PV systems: Modeling and approach of control," International Journal of Photoenergy, vol. 2019, 2019.
[25] A. Masnabadi, M. Asadi, M. Karimadini, and G. Dehnavi, "A Robust Control of a High-Power Isolated Battery Charger with Current Sharing Capability Under Transformer Parameters Uncertainty," Iranian Journal of Science and Technology, Transactions of Electrical Engineering, pp. 1-12, 2021.
[26] M. Gholizadeh and F. R. Salmasi, "Estimation of state of charge, unknown nonlinearities, and state of health of a lithium-ion battery based on a comprehensive unobservable model," IEEE Transactions on Industrial Electronics, vol. 61, no. 3, pp. 1335-1344, 2013.

Abolfazl Masnabadi was born in Iran, 1994. He received his B.S. and M.S. degrees in 2016 and 2018 at Arak University of Technology, Arak, Iran. His research interests are power electronics, DC/DC and DC/AC converter modeling and control and electrical machine drives.

Mehdi Asadi was born in Iran, 1979. He received B.Sc., M.Sc., and Ph.D. degrees in electrical engineering from Iran University of Science and Technology (IUST), Tehran, Iran in 2002, 2004, and 2013, respectively. Since 2013, he has jointed to the Arak University of Technology, Arak, Iran. His research interests include high powe and high frequency converters, Electrical machines drives, Power quality, Battery chargers, and FACTS devices.